PNAS RESEARCH ARTICLE | NEUROSCIENCE

Two intrinsic timing mechanisms set start and end times for dendritic arborization of a nociceptive neuron

Nobuko Suzuki[a], Yan Zou[a,b], HaoSheng Sun[c], Kelsie Eichel[d,e], Meiyu Shao[b], Mushaine Shih[a], Kang Shen[d,e], and Chieh Chang[a,1]

Edited by Yishi Jin, University of California, San Diego, La Jolla, CA; received June 15, 2022; accepted October 4, 2022

Choreographic dendritic arborization takes place within a defined time frame, but the timing mechanism is currently not known. Here, we report that the precisely timed *lin-4-lin-14* regulatory circuit triggers an initial dendritic growth activity, whereas the precisely timed *lin-28-let-7-lin-41* regulatory circuit signals a subsequent developmental decline in dendritic growth ability, hence restricting dendritic arborization within a set time frame. Loss-of-function mutations in the *lin-4* microRNA gene cause limited dendritic outgrowth, whereas loss-of-function mutations in its direct target, the *lin-14* transcription factor gene, cause precocious and excessive outgrowth. In contrast, loss-of-function mutations in the *let-7* microRNA gene prevent a developmental decline in dendritic growth ability, whereas loss-of-function mutations in its direct target, the *lin-41* tripartite motif protein gene, cause further decline. *lin-4* and *let-7* regulatory circuits are expressed in the right place at the right time to set start and end times for dendritic arborization. Replacing the *lin-4* upstream cis-regulatory sequence at the *lin-4* locus with a late-onset *let-7* upstream cis-regulatory sequence delays dendrite arborization, whereas replacing the *let-7* upstream cis-regulatory sequence at the *let-7* locus with an early-onset *lin-4* upstream cis-regulatory sequence causes a precocious decline in dendritic growth ability. Our results indicate that the *lin-4-lin-14* and the *lin-28-let-7-lin-41* regulatory circuits control the timing of dendrite arborization through antagonistic regulation of the DMA-1 receptor level on dendrites. The LIN-14 transcription factor likely directly represses *dma-1* gene expression through a transcriptional means, whereas the LIN-41 tripartite motif protein likely indirectly promotes *dma-1* gene expression through a posttranscriptional means.

lin-4-lin-14 pathway | *lin-28-let-7-lin-41* pathway | heterochronic genes | neuronal timers | dendrite arborization

Significance

Studies on the temporal control of cyclical processes such as circadian rhythm have frequently converged on the concept of biological oscillators, which act as intrinsic clocks that are resilient to changes in external environments. Understanding molecular oscillators gives a glimpse into temporal control for the cyclical nature of these processes. However, the timing mechanism for noncyclical processes, such as the differentiation of neurons into complex structures, is less well understood. In this study, we discover a role for the *lin-4-lin-14* and the *lin-28-let-7-lin-41* regulatory circuits in the control of start and end times for dendritic arborization.

Studies on the temporal control of cell cycle progression, circadian rhythm, and segmentation have frequently converged on the concept of biological oscillators (1–14). Biological oscillators are systems of molecules with various levels of expression and activity that act as clocks that determine biological rhythms resilient to changes in external environments. Understanding molecular oscillators gives a glimpse into temporal control for the cyclical nature of these processes. However, timing control for noncyclical biological processes is less understood. Most noncyclical events in nonneuronal cells are transient, which makes it difficult to study their temporal regulation. In contrast, differentiation of neurons into complex structures occurs on longer timescales, thereby giving us a window to peek into noncyclical mechanisms that control start and end times for dendritic arborization.

Although abundant knowledge has been learned in past decades on the temporal control of cell fate specification of neurons (15–17), less is known about the timing of their wiring to give rise to complex neuronal circuits and the timing of their plasticity. The heterochronic pathways are important temporal regulators of animal development and involve a number of microRNA-regulated posttranscriptional genetic circuits, including important interactions between the *lin-4* microRNA and its direct target, the *lin-14* transcription factor gene (18–20), and between the *let-7* microRNA and its direct target, the *lin-41* tripartite motif (TRIM) protein gene (21–23). Since the discovery of the *lin-4-lin-14* and the *let-7-lin-41* regulatory circuits broadly expressed in the nervous system (24–26), evidences indicating a widespread role of the *lin-4-lin-14* and the *let-7-lin-41* regulatory circuits in timing neuronal assembly and plasticity start to emerge. The *lin-4* microRNA and the LIN-14 transcription factor regulate the temporal transition of sequential events in anterior ventral microtubule (AVM) neuronal connectivity. Up-regulation of *lin-4* and down-regulation of *lin-14* signal the end of netrin-mediated axon pathfinding to allow synapse formation in AVM neurons (24, 27). *lin-4* and *lin-14* are also involved in the temporal control of axon pathfinding in other neurons (28, 29) as well as synaptic rewiring of motor neurons (30, 31). Additionally, *lin-14* temporally

Author affiliations: [a]Department of Biological Sciences, University of Illinois at Chicago, Chicago, IL 60607; [b]School of Life Science and Technology, ShanghaiTech University, Shanghai 201210, China; [c]Department of Cell, Developmental and Integrative Biology, University of Alabama at Birmingham, Birmingham, AL 35233; [d]HHMI, Stanford University, Stanford, CA 94305; and [e]Department of Biology, Stanford University, Stanford, CA 94305

Author contributions: N.S., Y.Z., H.S., K.E., M. Shih., M. Shao, K.S., and C.C. designed research; N.S., Y.Z., H.S., K.E., M. Shao, and M. Shih performed research; H.S., K.E., and K.S. contributed new reagents/analytic tools; N.S., Y.Z., H.S., M. Shao, M. Shih, and C.C. analyzed data; and N.S., K.S., and C.C. wrote the paper.

The authors declare no competing interest.

This article is a PNAS Direct Submission.

[1]To whom correspondence may be addressed. Email: chieh.chang1@gmail.com.

This article contains supporting information online at http://www.pnas.org/lookup/suppl/doi:10.1073/pnas.2210053119/-/DCSupplemental.

Published November 2, 2022.

regulates the onset of *zig* gene expression to maintain ventral nerve cord structure (32). The *let-7* microRNA and the LIN-41 tripartite motif protein control the timing of a postdifferentiation event in AVM neurons (25, 33). The progressive increase of *let-7* and the progressive decrease of *lin-41* contribute to a normal developmental decline in AVM axon regeneration. Both *lin-4* and *let-7* microRNAs regulate axodendritic polarity in the DA9 motor neuron (34). Despite advances in understanding of the temporal transition of neuronal connectivity and regeneration decline, it is still unknown how neurons set not only start but also end times of developing a complex neuronal structure. Using the CRISPR technology, we successfully manipulated the timing of *lin-4* and *let-7* expression by swapping their upstream cis-regulatory sequences with each other. In this way, we can turn back the clock in old neurons and turn forward the clock in young neurons to demonstrate that the two timing regulatory circuits restrict dendritic arborization within a defined time frame.

Dendritic arborization of the posterior ventral process D (PVD) nociceptive neurons takes place within a defined time period starting at the second larval (L2) stage and ending at the young adult stage during *Caenorhabditis elegans* development. The PVD dendritic arbor is established by a complex but well-ordered array of nonoverlapping sister dendrites. The creation of this structure involves a sequential series of branching decisions, which makes PVD neurons an ideal model system to study timing mechanisms of dendritic arborization. A 1° dendrite extends from the PVD cell body along the anterior/posterior axis at the location of the lateral nerve fascicle. Orthogonal arrays of 2°, 3°, and 4° dendritic branches envelop the animal in a manner that alternates between the dorsal/ventral and the anterior/posterior axis to produce an elaborate network of sensory processes (35, 36). The well-ordered dendrite branches are structurally likened to menorahs, which are branched candle holders. The growth of these dendrite branches depends on the DMA-1 dendrite receptor in PVD neurons (37). What timing mechanisms initiate and terminate the arborization of this complex dendritic structure? To answer these questions, we search for molecules in PVD neurons that may provide intrinsic temporal control of dendritic arborization. We identify two timing regulatory circuits that restrain the growth of PVD dendrites within a set time frame. The initial dendritic outgrowth in PVD neurons is actuated by the precisely timed *lin-4-lin-14* regulatory circuit, which positively and likely directly modulates the DMA-1 dendrite receptor level through a transcriptional means. The dendritic growth is subsequently slowed down by the precisely timed *lin-28-let-7-lin-41* regulatory circuit, which negatively and likely indirectly modulates the DMA-1 dendrite receptor level through a post-transcriptional means, as dendritic arborization comes to an end.

Results

***lin-4* and *let-7* Are Temporally Expressed in PVD Neurons during Dendrite Arborization.** To identify timing mechanisms that restrict PVD dendritic arborization within a defined time period, we sought to identify molecules that are expressed in PVD neurons and whose expression coincides with start and end times of PVD dendritic arborization. We discovered *lin-4* and *let-7* microRNAs to be excellent candidates that fit both criteria. To understand the temporal control of *lin-4* and *let-7* gene expression in PVD neurons, we developed a *lin-4* reporter by fusing a 1.9-kb upstream region of a mature *lin-4* microRNA to the GFP gene and a *let-7* reporter by fusing a 2.9-kb upstream region of mature *let-7* microRNA to the GFP gene and confirmed that they both were stably expressed in PVD (Fig. 1 and *SI Appendix*, Fig. S1). The expression levels of these two reporters in the whole animal at different developmental stages correlated strongly with the whole animal stem-loop RT-PCR quantification of *lin-4* and *let-7* microRNAs, indicating that these two reporters are reliable. Using these reporters, we determined the timing of *lin-4* and *let-7* expression in PVD neurons during dendritic arborization (Fig. 1 *D*–*G*). The *lin-4* reporter was expressed highly in PVD at the late L2-the early third larval (L3) stage, when the secondary dendrites start elaborating (Fig. 1 *A*, *B*, *D*, and *F*). In contrast, the *let-7* reporter was expressed at relatively low levels in PVD at the L3 stage but was significantly elevated from the L4 stage onwards, when the growth of the terminal quaternary dendrites comes to an end (Fig. 1 *A*, *C*, *E*, and *G*). These results indicate that *lin-4* and *let-7* are expressed in the right place at the right time to initiate and terminate PVD dendritic arborization, respectively.

The *lin-4-lin-14* Regulatory Circuit Initiates Dendritic Outgrowth in PVD Neurons. We previously reported that the *lin-4* microRNA represses the expression of the LIN-14 transcription factor to inhibit AVM axon attraction (24, 27). Further analysis of *lin-4* and *lin-14* reporters revealed an overlapping expression of two genes in many other neurons, including PVD, at the early L3 stage (Fig. 1*B* and *SI Appendix*, Fig. S1 *A*–*C*), when PVD neurons are sending out the secondary dendrites. We showed that *lin-4(e912)* loss-of-function *(lf)* and *lin-14(n355)* gain-of-function *(gf)* mutants displayed a similar phenotype of limited dendritic outgrowth in PVD neurons (Fig. 2 *A*–*C* and *E*). In both *lin-4(e912lf)* and *lin-14(n355gf)* mutants, the frequencies of the PVD secondary branches at the young adult stage were 30 to 40% lower compared with that in the wild type ($n > 20$ analyzed in each strain). In addition, PVD neurons in the majority of *lin-4(e912lf)* and *lin-14(n355gf)* mutants entirely lacked the tertiary branches even at the young adult stage, although subsets of PVD neurons in these mutants displayed a small number of tertiary branches in the area close to the cell body. These results suggest that the *lin-4* microRNA may inhibit the expression of the LIN-14 transcription factor to initiate dendrite outgrowth. Consistent with this interpretation, reduced *lin-14* activity caused opposite effects. In wild-type animals at the mid-L3 stage, PVD dendrites can only grow up to the tertiary branch (Fig. 2*F*). However, in *lin-14(n179)* reduction-of-function (*rf*) mutants at the same developmental stage, the mid-L3 stage, PVD dendrites can grow up to the quaternary branch and complete the menorah structure (Fig. 2*F*), suggesting precocious dendrite outgrowth. In addition, the number of overlapped tertiary dendrites caused by excessive tertiary dendrite growth was significantly higher in *lin-14(n179rf)* mutants than in wild-type animals at the young adult stage (Fig. 2 *A*, *D*, and *G* and *SI Appendix*, Fig. S2). Thus, a reduction of function in the *lin-14* gene causes precocious and excessive dendritic outgrowth. The *lin-14(n179rf)* mutant phenotype of excessive PVD tertiary dendrite growth can be rescued by re-expressing the *lin-14* gene in PVD neurons, suggesting that *lin-14* acts cell-autonomously in PVD (Fig. 2*G*). To further strengthen the statement that the *lin-4* microRNA targets the *lin-14* transcription factor to initiate dendritic outgrowth in PVD neurons, we tested whether the *lin-14(n179rf)* mutation suppresses the *lin-4(e912lf)* mutant phenotype of delayed dendritic outgrowth. We found that this is indeed the case (Fig. 2*F*). *lin-4(lf); lin-14(rf)* double mutants displayed the same precocious dendritic outgrowth phenotype of the *lin-14(n179rf)* single mutant rather than delayed dendritic outgrowth phenotypes of the *lin-4(lf)* single mutant (Fig. 2*F*). Taken together, our results indicate that the *lin-4-lin-14* regulatory circuit initiates dendritic outgrowth in PVD neurons.

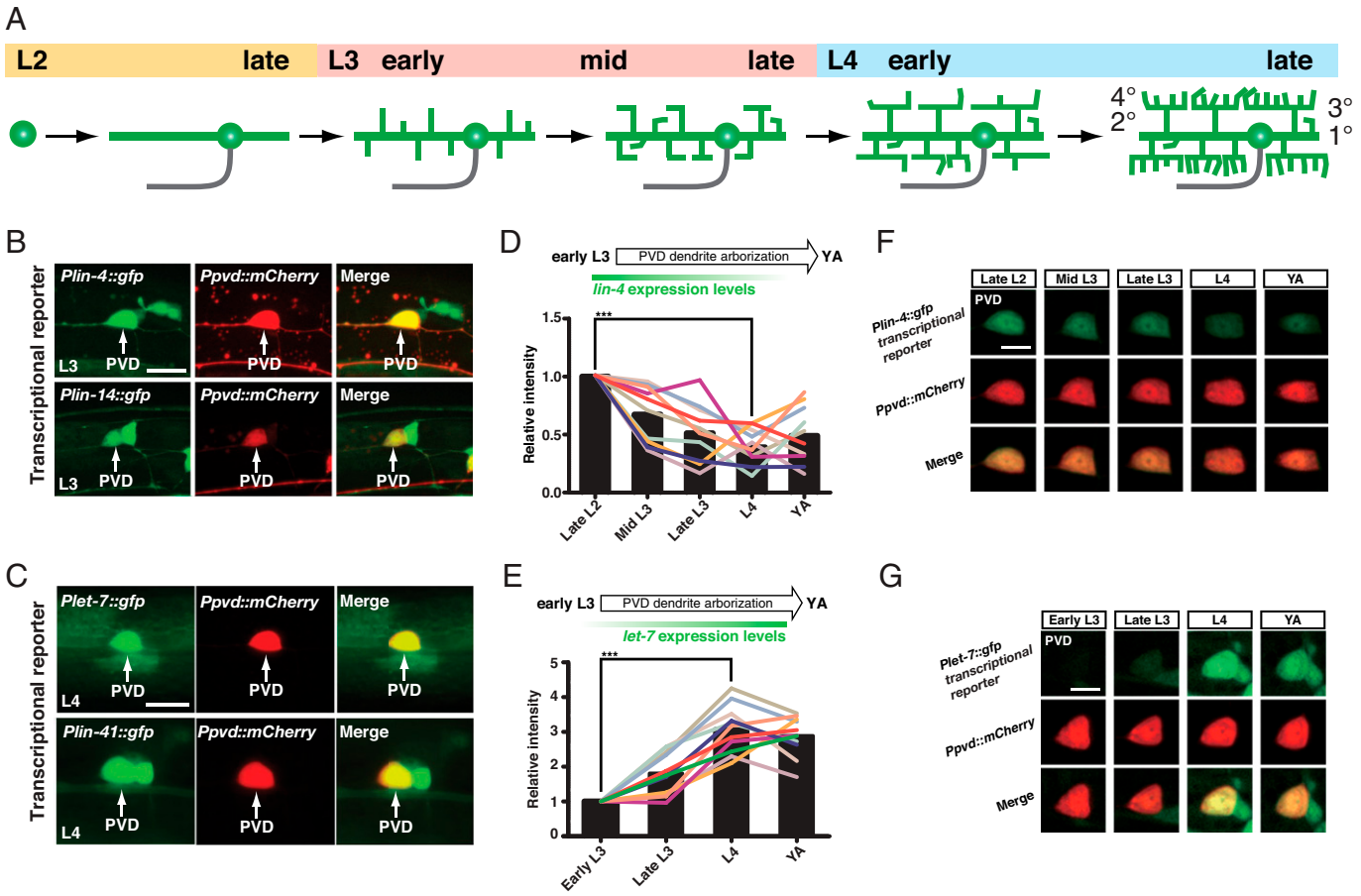

Fig. 1. Expression of *lin-4/lin-14* and *let-7/lin-41* regulatory circuits in PVD neurons. (*A*) The timing and steps of PVD dendrite arborization. Schematic drawings of PVD dendrite arbors at different stages of development, late L2 to late L4. All views showing the *Left*-side cells of each PVD pair; anterior is to the *Left*. A single axon (gray color) emerges ventralward from the cell body before traveling anteriorly along the ventral nerve cord. The dendrite processes emerging from the cell body elaborate into highly organized dendrite arbors. (*B*) Both *Plin-4::GFP* and *Plin-14::GFP* transcriptional reporters are expressed in PVD neurons. (*C*) Detection of both *Plet-7::GFP* and *Plin-41::GFP* transcriptional reporter expression in PVD neurons. Scale bar, 10 μm. (*D*) Expression of the *Plin-4::GFP* reporter in PVD neurons was assessed at five different stages of development based on the GFP fluorescence intensity in the cell body. (*E*) Expression of the *Plet-7::GFP* reporter in PVD neurons was assessed at four different stages of development based on the GFP fluorescence intensity in the cell body. Each line represents data from a single animal followed over time. Bars represent the average expression intensity of either the *Plin-4::GFP* or the *Plet-7::GFP* reporter measured at each time point. ***$P < 0.001$ by a Student's *t* test. YA, the young adult stage. (*F* and *G*) Time-lapse imaging of the *Plin-4::GFP* and the *Plet-7::GFP* reporter expression in PVD neurons at different stages of development. The *PF49H12.4::mCherry* reporter was used to label PVD neurons. Scale bar, 5 μm. See also *SI Appendix*, Fig. S1.

The *let-7-lin-41* Regulatory Circuit Slows Down Dendrite Growth in the Final Stage of Dendrite Arborization. We previously reported that the *let-7* microRNA represses the expression of the LIN-41 tripartite motif protein to inhibit AVM axon regeneration in older neurons (25, 33). Here, we further studied the expression of *let-7* and *lin-41* reporters and found an overlapping expression of the two genes in many other neurons, including PVD, at the L4 stage (Fig. 1*C* and *SI Appendix*, Fig. S1 *D–F*), when the growth of the terminal quaternary dendrites in PVD comes to an end. We performed laser dendritomy on the primary dendrite in PVD neurons at the L3, young adult, and day one into the adult (the D1 A) stages. Dendrite regrowth in each animal was measured 24 h after dendritomy throughout this study. We found that PVD dendritic growth ability is significantly lower at the adult stage than at the L3 stage (Fig. 3 *A*, *B*, and *E*), suggesting that PVD neurons undergo a developmental decline in dendritic growth ability. Our expression analysis showed that the *let-7* expression in PVD was at relatively low levels at the L3 stage but was significantly elevated from the L4 stage onwards, which implicates its contribution to the developmental decline in PVD dendritic growth ability (Fig. 1 *E* and *G*). Indeed, the dendritic growth ability in adult *let-7* mutants was indistinguishable from that seen in wild-type animals at an earlier developmental stage, the L3 stage (Fig. 3 *A–E*), suggesting that *let-7* mutations may retard a normal developmental decline in dendritic growth ability. In the young adult stage, while the *let-7(n2853rf)* mutation significantly enhanced, the *lin-41(n2914lf)* mutation significantly reduced dendritic growth ability in PVD neurons (Fig. 3*F*). In addition, *lin-41* mutations suppressed the *let-7(n2853rf)* mutant phenotype of enhancing dendrite growth ability at the young adult stage, suggesting that the *let-7* microRNA targets the LIN-41 tripartite motif protein to inhibit dendrite growth in PVD neurons (Fig. 3*F*). Together, these results indicate that the *let-7-lin-41* regulatory circuit slows down dendrite growth in the final stage of dendrite arborization.

***lin-28* Inhibits the *let-7-lin-41* Circuit to Regulate the Timing of Dendrite Arborization.** Previous studies have shown that the LIN-28 RNA-binding protein blocks the maturation of the *let-7* microRNA in both invertebrates and vertebrates (38–41). We found that a *lin-28::GFP* fosmid-based reporter, which contains the *lin-28* upstream cis-regulatory, exonic, intronic, and downstream cis-regulatory sequences, is expressed in PVD neurons (Fig. 3*G*). To determine whether *lin-28* acts upstream of *let-7* to regulate the timing of PVD dendrite arborization, we first compared the endogenous LIN-41 protein level in PVD neurons between

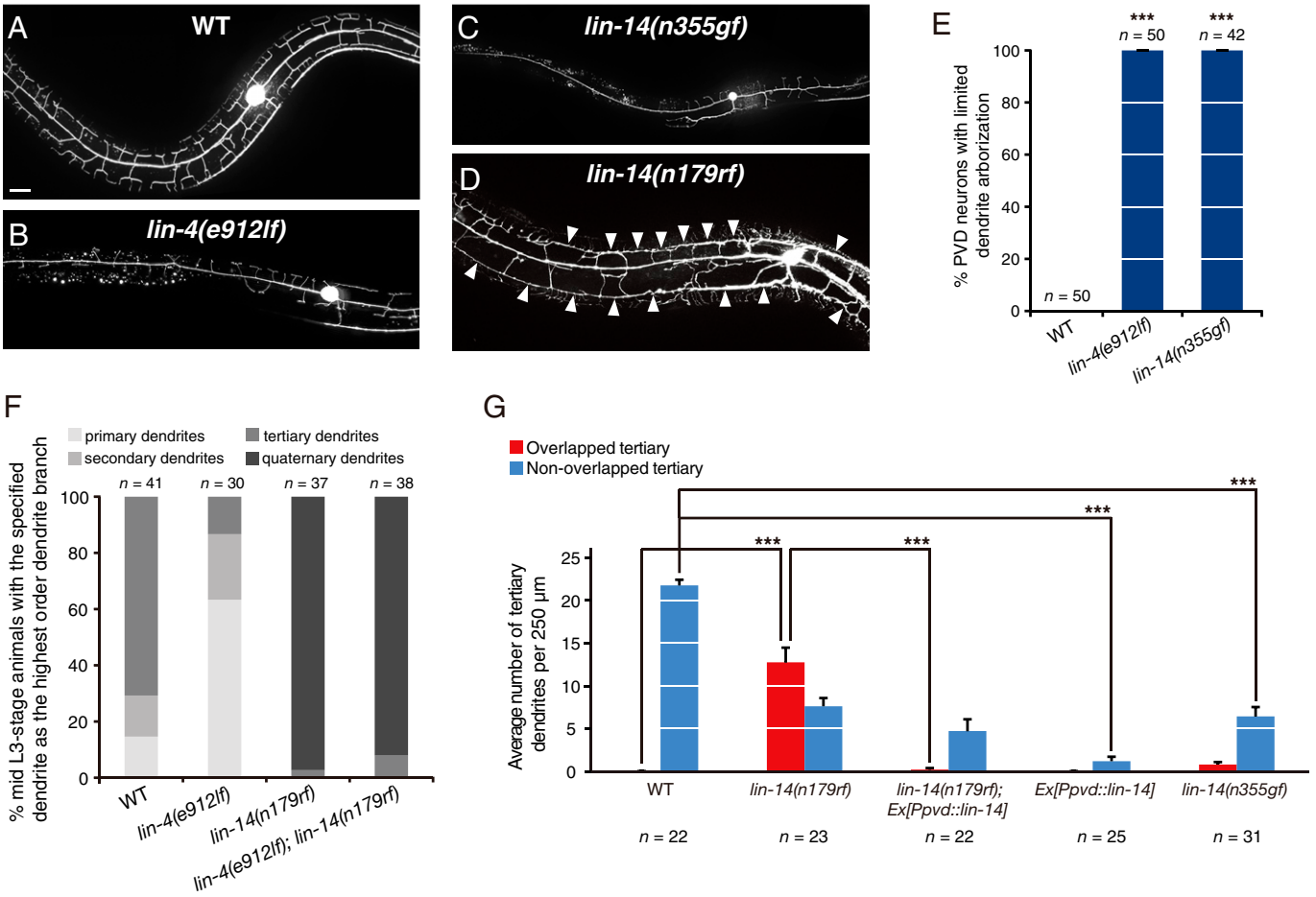

Fig. 2. Initiation of dendritic arborization is affected by mutations in the *lin-4-lin-14* regulatory circuit. (*A–D*) Representative images showing the extent of dendrite arborization in the wild type and *lin-4(e912lf)*, *lin-14(n355gf)*, and *lin-14(n179rf)* mutants at the young adult stage. Arrowheads point to contacts between neighboring tertiary dendrites. Scale bar, 20 µm. WT, wild type. (*E*) Percentages of PVD neurons at the young adult stage with limited dendrite outgrowth in the wild type, *lin-4(e912lf)*, and *lin-14(n355gf)* mutants. Error bars, Standard Error of the Proportion (SEP). ***$P < 0.001$, relative to the wild type, by a two-proportion *Z*-test. (*F*) Percentages of PVD neurons at the mid-L3 stage based on the highest order dendrite branch observed in the wild type and *lin-4(e912lf)*, *lin-14(n179rf)*, and *lin-4(e912lf); lin-14(n179rf)* mutants. (*G*) Quantification of the number of tertiary branches per 250 µm in the anterior direction from the PVD cell body at the young adult stage. Tertiary dendrites were divided into two groups, as follows: nonoverlapped tertiary is defined as those with normal self-avoidance and overlapped tertiary as those with self-avoidance defects. All strains were raised at 25 °C, which is nonpermissive temperature for the *lin-14(n179)* allele. Error bars, SEM. ***$P < 0.001$ by one-way ANOVA with Tukey's test. See also *SI Appendix*, Fig. S2.

the wild type and *lin-28(n719lf)* mutants. The mNG reporter gene was knocked in the endogenous *lin-41* locus to generate a *mNG::lin-41* fusion gene using the CRISPR-Cas9 technology (26). We found that the *lin-28(n719lf)* mutation significantly reduced LIN-41 protein levels in PVD neurons compared with the wild type at the early L3 stage (Fig. 3 *H* and *I*), suggesting that *lin-28* inhibits the *let-7-lin-41* circuit in PVD neurons. We performed laser dendritomy on PVD primary dendrites in *lin-28(n719lf)* mutants at the young adult stage and observed a significantly reduced dendrite growth ability in *lin-28 (n719lf)* mutants compared with wild-type animals at the same stage 24 h after surgery (Fig. 3*J*), a phenotype that is opposite to the *let-7(n2853rf)* mutant phenotype of enhanced dendrite growth ability (Fig. 3*F*). Furthermore, *lin-41* overexpression in PVD neurons significantly suppressed the *lin-28(n719lf)* mutant phenotype of reduced dendrite growth ability (Fig. 3*J*). Together, these results support that *lin-28* inhibits the *let-7-lin-41* circuit to regulate the timing of PVD dendrite arborization.

Recent studies in sexually dimorphic nervous system differentiation and male tail tip morphogenesis revealed that the *lep-5* long noncoding RNA (lncRNA) promotes degradation of LIN-28 (42, 43). To determine whether *lep-5* plays a role in regulating the *lin-28-let-7-lin-41* regulatory circuit in PVD neurons, we first analyzed the endogenous LIN-41 protein level in PVD neurons in the wild type versus *lep-5(ny28lf)* mutants. We found there is no difference of LIN-41 protein levels in PVD neurons between the wild type and *lep-5(ny28lf)* mutants (*SI Appendix*, Fig. S3 *A* and *B*). In addition, *lep-5(ny28lf)* mutants displayed a similar extent of dendrite growth ability to wild-type animals at the young adult stage (*SI Appendix*, Fig. S3*C*). Thus, *lep-5* is unlikely to regulate the timing of PVD dendrite arborization by modulating the *lin-28-let-7-lin-41* circuit.

The *lin-4* to *let-7* Upstream Sequence Replacement Delays Dendrite Arborization. To further support our conclusion that *lin-4* and *let-7* microRNAs set start and end times for PVD dendrite arborization, we manipulated the timing of their expression by swapping their upstream sequences with each other. We found that the delayed expression of *lin-4* (*lin-4* microRNA expressed from the *let-7* upstream sequence from the L3 stage onwards) postponed dendrite arborization in PVD neurons (*SI Appendix*, Fig. S4). The transgene that expressed the *lin-4* microRNA from the *let-7* upstream sequence (*let-7up::lin-4*) led to retarded growth in quaternary dendrites (the final order of PVD

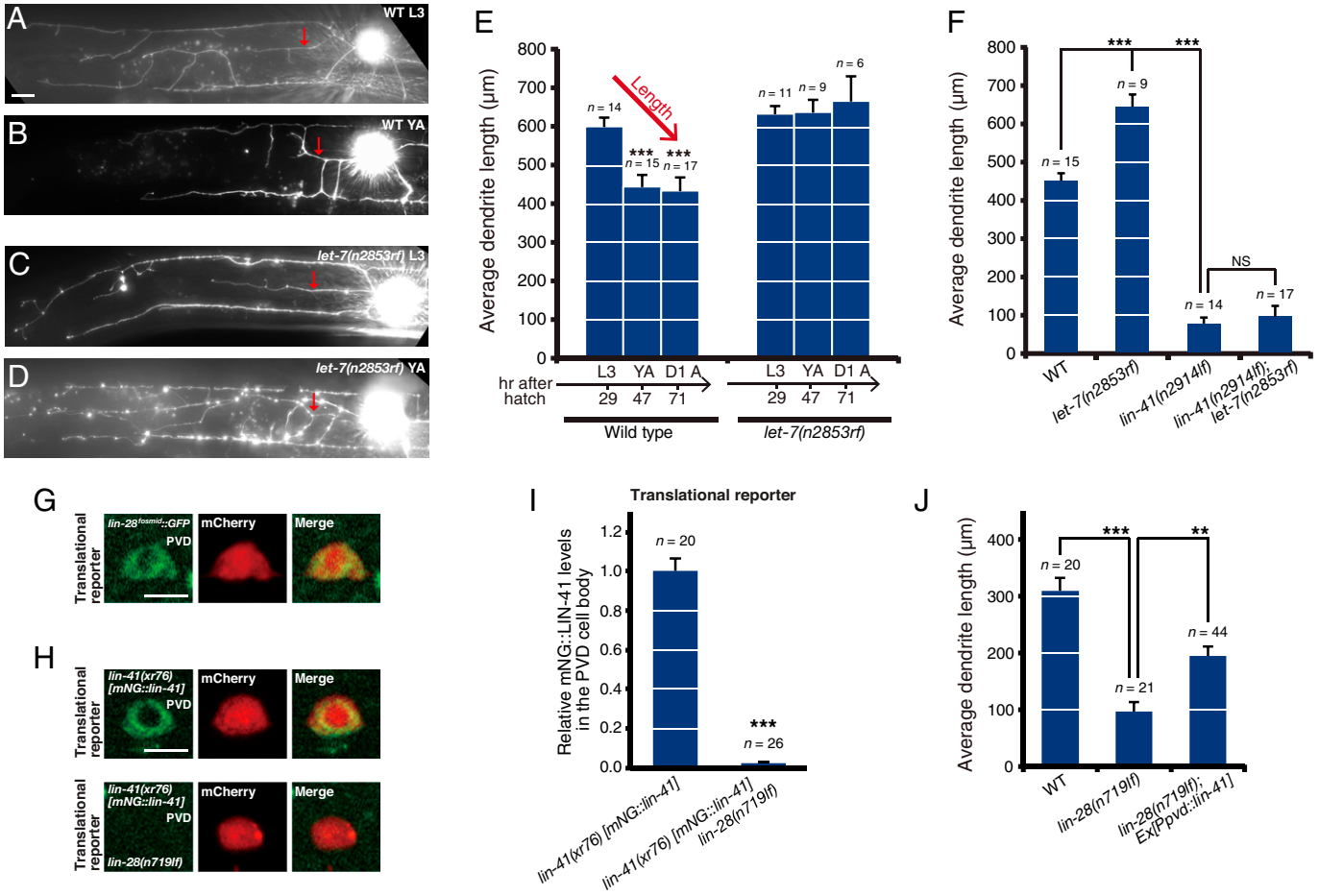

Fig. 3. Developmental decline in dendrite growth ability is affected by mutations in the *lin-28-let-7-lin-41* regulatory circuit. (*A–D*) Representative images showing the extent of dendrite regrowth 24 h after dendritomy of the primary dendrite in PVD at either the L3 or the young adult stage in wild type (*A* and *B*) and *let-7(n2853rf)* mutants (*C* and *D*). PVD dendrites were visualized using the *xrIs37[PF49H12.4::GFP]* marker. Dorsal is *Up*; anterior is to the *Left*. Red arrows indicate lesion sites. Scale bar, 20 μm. (*E*) Average PVD dendrite length regrown in wild type and *let-7(n2853rf)* mutants 24 h following dendritomy at different stages. Asterisks indicate cases in which later-stage animals differ from L3-stage animals at ***$P < 0.001$ by a Student's *t* test. D1 A, day one into the adult stage. Error bars, SEM. (*F*) Average PVD dendrite length regrown in various strains 24 h following dendritomy at the young adult stage. Asterisks indicate cases in which *let-7* or *lin-41* mutants differ from wild type at ***$P < 0.001$ by one-way ANOVA with Tukey's test. NS, not significant. All animals including the *let-7(n2853rf)* allele were raised and analyzed at 20 °C. *let-7(n2853rf)* mutants were quantified only in those that survived bursting vulva. (*G*) Representative images of LIN-28 protein expression in PVD neurons in the wild type at the early L3 stage. A *lin-28::GFP* fosmid-based reporter was analyzed. The *Pser-2::mCherry* reporter was used to label PVD neurons. Scale bar, 5 μm. (*H*) Representative images of endogenous LIN-41 protein expression in PVD neurons in the wild type and *lin-28(n719lf)* mutants at the early L3 stage. Scale bar, 5 μm. (*I*) Quantification of LIN-41 proteins based on the mNG::LIN-41 fluorescence intensity in the PVD cell body in the wild type and *lin-28(n719lf)* mutants. Error bars, SEM. ***$P < 0.001$ by a Student's *t* test. (*J*) Average PVD dendrite length regrown in various strains 24 h following dendritomy at the young adult stage. Error bars, SEM. **$P < 0.01$ and ***$P < 0.001$ by one-way ANOVA with Tukey's test.

dendrites) in *lin-4 lf* mutants at the L3 molt and the early L4 stage (*SI Appendix*, Fig. S4 *A* and *B*). However, the growth of quaternary dendrites in these transgenic animals (*lin-4(e912lf); Ex[let-7up::lin-4]*) was able to catch up later in the adult stage (*SI Appendix*, Fig. S4*C*). To further strengthen this conclusion, we utilized the CRISPR-Cas9 technology to replace the endogenous *lin-4* upstream sequence at the *lin-4* locus with a late-onset *let-7* upstream sequence (Fig. 4*A*). The repair templates that have been developed recently were used to facilitate the identification of the CRISPR recombinants (44, 45) *lin-4(xr70)* and *lin-4(xr71)* in which the endogenous *lin-4* upstream sequence has been replaced by a *let-7* upstream sequence. We used stem-loop and TaqMan real-time RT-PCR to globally survey the temporal expression of mature *lin-4* microRNA during animal development. Expression of the *lin-4* microRNA in the *lin-4* to *let-7* upstream sequence replacement CRISPR allele was indeed delayed compared with its expression in wild-type animals (Fig. 4 *A* and *B* and *SI Appendix*, Fig. S5*A*). In these CRISPR lines, *lin-4(xr70)* and *lin-4(xr71)*, we observed retarded growth of the quaternary dendrites at the early L4 stage (green dots in Fig. 4*E* compared with Fig. 4*C* of the wild type; Fig. 4*G*), which was able to catch up later in the adult stage (green dots in Fig. 4*F* compared with Fig. 4*D* of the wild type; Fig. 4 *H–J*). These results demonstrate that by manipulating the timing of *lin-4* expression through the *lin-4* to *let-7* upstream sequence replacement we can delay dendrite arborization.

The *let-7* to *lin-4* Upstream Sequence Replacement Precociously Inhibits Dendrite Growth Ability. Conversely, the premature expression of *let-7* (*let-7* microRNA expressed from the *lin-4* upstream sequence from the L1 stage onward) precociously inhibited dendritic growth ability in PVD neurons (Fig. 5 *A–C*). We utilized the CRISPR-Cas9 technology to generate the *let-7(xr67)* CRISPR line in which the endogenous *let-7* upstream sequence at the *let-7* locus has been replaced with an early-onset *lin-4* upstream sequence (Fig. 5*A*). Stem-loop and TaqMan real-time RT-PCR analysis showed that the expression of mature *let-7* microRNA in the *let-7* to *lin-4* upstream

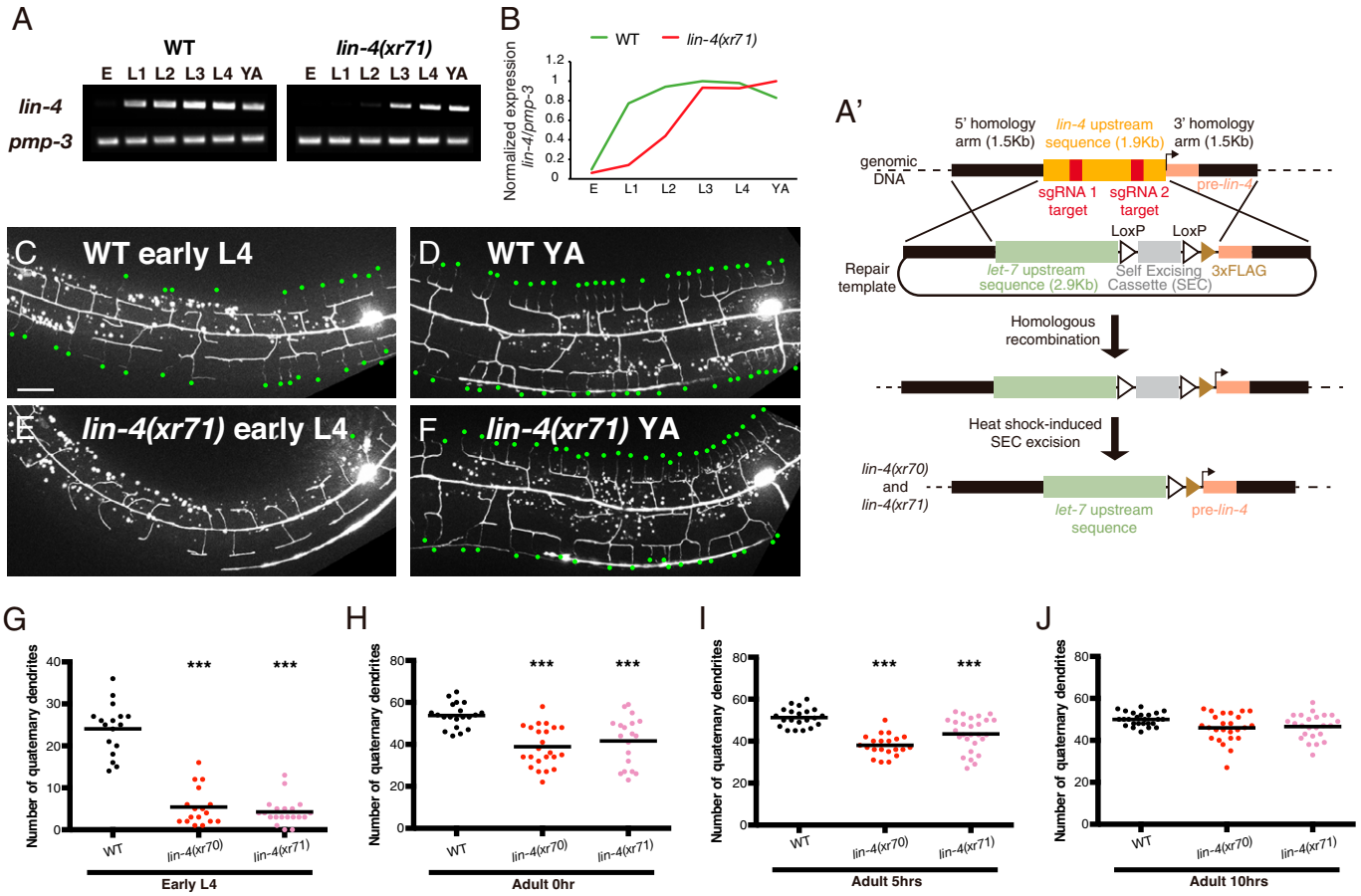

Fig. 4. Delayed dendrite arborization by the *lin-4* to *let-7* upstream sequence replacement. Expression of the *lin-4* microRNA by a late-onset *let-7* upstream sequence postponed the growth of the quaternary dendrites. (*A*) Stem-loop RT-PCR analysis of RNA isolated from populations of staged animals revealed late-onset expression of the *lin-4* microRNA in the *lin-4(xr71)* CRISPR line in contrast to early-onset expression in wild-type animals. (*A'*) Strategies of upstream sequence replacements by the CRISPR-Cas9 technology. In this upstream sequence swap experiment, we swapped the 1.9-kb sequence upstream of *lin-4* pre-miRNA with the 2.9-kb sequence upstream of *let-7* pre-miRNA. So in the resulting *let-7* upstream sequence::*lin-4* configuration, the *let-7* upstream sequence (includes *let-7* promoter and *let-7* primary sequence minus *let-7* pre and mature miRNA sequence) contains new temporal information for both driving *lin-4* expression and processing primary *lin-4*. (*B*) The progressive change of mature *lin-4* microRNA expression in the wild type and the *lin-4(xr71)* CRISPR line during development was determined by measuring the mature *lin-4* microRNA level normalized by the *pmp-3* level generated from stem-loop and regular RT-PCRs, respectively. (*C–F*) Representative images showing the extent of quaternary dendrite arborization in the wild type (*C* and *D*) and the *lin-4(xr71)* CRISPR line (*E* and *F*), in which the endogenous *lin-4* upstream sequence has been replaced by the *let-7* upstream sequence. Images were taken at the early L4 (*C* and *E*) and the young adult (*D* and *F*) stages. Dorsal is *Up*; anterior is to the *Left*. Green dots indicate quaternary dendrites. Scale bar, 20 μm. (*G–J*) Quantification of the number of quaternary branches per 250 μm in the anterior direction from the PVD cell body at the early L4 stage (*G*) or various time points at the young adult stage (*H–J*) in the wild type and *lin-4(xr70)* and *lin-4(xr71)* CRISPR lines. Each dot represents data from a single animal. ***$P < 0.001$ by one-way ANOVA with Dunnett's test. See also *SI Appendix*, Figs. S4 and S5.

sequence replacement CRISPR line was indeed precocious compared with its expression in wild-type animals (Fig. 5 *A* and *B* and *SI Appendix*, Fig. S5*B*). In the *let-7(xr67)* CRISPR line, PVD dendrite growth ability at the L3 stage was significantly lower than that in wild-type animals at the same stage (L3) and similar to that in wild-type animals at an older stage (young adult) (Fig. 5*C*). PVD dendrite growth ability in the *let-7(xr67)* line was further reduced at the young adult stage (Fig. 5*C*). Interestingly, PVD dendrites, both proximal and distal segments to the injured site, in *let-7(xr67)* animals degenerated 24 h following laser dendritomy at the D1 A stage. Because of this, we were unable to determine the dendrite growth ability at the D1 A stage (Fig. 5*C*). Thus, by manipulating the timing of *let-7* expression through the *let-7* to *lin-4* upstream sequence replacement, we can precociously inhibit dendrite growth ability. Taken together, these findings support a model in which the *lin-4-lin-14* regulatory circuit sets the start time, whereas the *let-7-lin-41* regulatory circuit sets the end time for PVD dendrite arborization (see Fig. 7*H*).

***lin-14* and *lin-41* Antagonistically Regulate the DMA-1 Receptor Level on PVD Dendrites.** Two transmembrane ligands, namely, SAX-7 and MNR-1, work together with LECT-2, a secreted ligand, to instruct dendrite arborization in PVD neurons through interactions with the dendrite receptor DMA-1 (37, 46–49). SAX-7, MNR-1, LECT-2, and DMA-1 form a multiprotein receptor–ligand signaling complex that directs the growth of stereotyped dendritic branches. Of these four components, only DMA-1 functions cell-autonomously in PVD neurons. One way to control dendrite growth ability during the course of PVD dendrite arborization is through the regulation of responsiveness of dendrites to growth signals, which can be accomplished by adjusting the abundance of the receptor on dendrites (50). In addition to DMA-1, HPO-30 can function cell-autonomously in PVD neurons as a coreceptor to regulate dendrite arborization by forming a signaling complex with DMA-1 (51–53). We ruled out *hpo-30* as a candidate target gene of the two microRNA regulatory circuits since the level of HPO-30 proteins on dendrites was not affected by *lin-14* and *lin-41* mutations, suggesting *hpo-30* is not regulated by

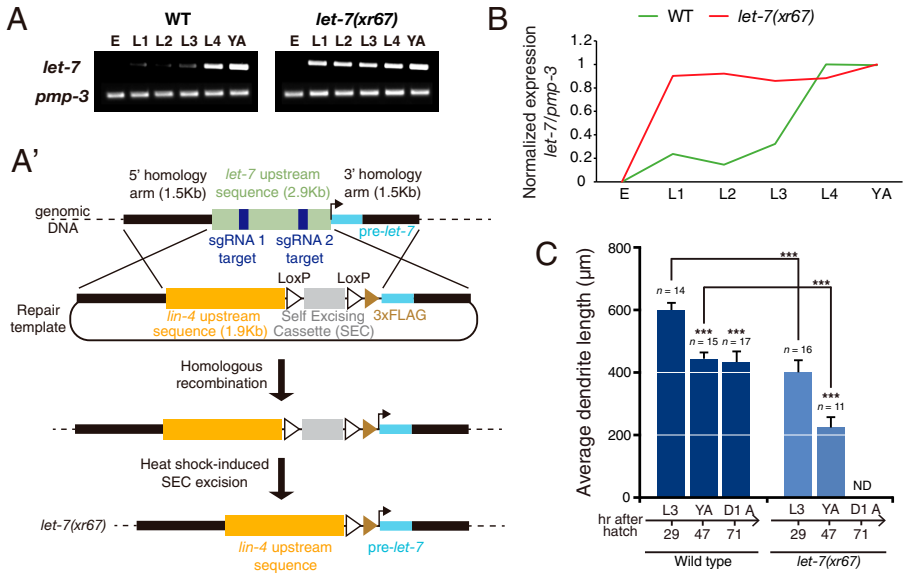

Fig. 5. Precocious decline in dendrite growth ability by the *let-7* to *lin-4* upstream sequence replacement. Expression of the *let-7* microRNA by an early-onset *lin-4* upstream sequence precociously reduced dendrite growth ability in PVD neurons. (*A*) Stem-loop RT-PCR analysis of RNA isolated from populations of staged animals revealed early-onset expression of the *let-7* microRNA in the *let-7(xr67)* CRISPR line contrast to late-onset expression in wild-type animals. (*A'*) Strategies of upstream sequence replacements by the CRISPR-Cas9 technology. In this upstream sequence swap experiment, we swapped the 2.9-kb sequence upstream of *let-7* pre-miRNA with the 1.9-kb sequence upstream of *lin-4* pre-miRNA. So in the resulting *lin-4* upstream sequence::*let-7* configuration, the *lin-4* upstream sequence (includes *lin-4* promoter and *lin-4* primary sequence minus *lin-4* pre and mature sequence), which likely resists LIN-28 RBP repression, contains new temporal information for both driving *let-7* expression and processing primary *let-7*. (*B*) The progressive change of mature *let-7* microRNA expression in the wild type and the *let-7(xr67)* CRISPR line during development was determined by measuring the mature *let-7* microRNA level normalized by the *pmp-3* level generated from stem-loop and regular RT-PCRs, respectively. (*C*) Average PVD dendrite length regrown in the wild type and the *let-7(xr67)* CRISPR line 24 h following dendritomy of the primary dendrite at different stages. Asterisks indicate cases in which later-stage animals differ from L3-stage animals or a comparison between the wild type and *let-7(xr67)* at the same stage is significantly different at ***$P < 0.001$ by a Student's *t* test. D1 A, day one into the adult stage. ND, not determined. Error bars, SEM. See also *SI Appendix*, Fig. S5.

lin-14 and *lin-41* (*SI Appendix*, Fig. S6 *A* and *B*). In contrast, the expression of DMA-1 proteins on dendrites appeared to be regulated by *lin-14* and *lin-41*. To analyze the endogenous level of DMA proteins on PVD dendrites, we knocked in a GFP reporter after the transmembrane domain of the endogenous *dma-1* gene using the CRISPR-Cas9 technology. This knock-in strain does not show any noticeable defects in PVD dendrites, suggesting that the *gfp* knock-in retains *dma-1* gene function. The endogenous DMA-1 protein level on PVD tertiary dendrites increased in the early stage of dendrite arborization, from the early L3 to early L4 stage, and decreased subsequently in the final stage of dendrite arborization, from the early L4 to the young adult stage, which correlates with a dynamic change in dendrite growth ability during dendrite arborization (Fig. 6*A*). This observation, combined with our results that two microRNA regulatory circuits set start and end times for PVD dendrite arborization, led us to hypothesize that the *lin-4-lin-14* and the *lin-28-let-7-lin-41* regulatory circuits control the timing of PVD dendrite arborization through antagonistic regulation of the DMA-1 protein level on dendrites (Fig. 6*B*).

To determine whether the *lin-4-lin-14* regulatory circuit controls the timing of PVD dendrite arborization through the regulation of the DMA-1 receptor level on PVD dendrites, we analyzed the level of DMA-1 proteins on tertiary dendrites in *lin-14(n179rf)* mutants versus wild-type animals. We found that the endogenous level of DMA-1 proteins based on the fluorescence intensity of DMA-1::GFP was significantly increased in *lin-14(n179rf)* mutants (Fig. 6 *C–E*), consistent with their higher dendrite growth ability (Fig. 2 *D* and *G*). This result suggests that *lin-14* negatively regulates *dma-1* expression in PVD neurons. To understand the mechanism by which *lin-14* negatively regulates the DMA-1 level on PVD dendrites, we engineered a *dma-1* transcriptional reporter by inserting the SL2 trans-splice site and the mNG reporter gene into the 3′ end of the endogenous *dma-1* gene using CRISPR-Cas9 technology. With the insertion of this SL2 trans-splice site between *dma-1* and *mNG*, even though they are cotranscribed, they can be translated separately, thus allowing us to read out the transcription of the *dma-1* gene based on the intensity of the mNG reporter (54). An analysis of the SL2-based *dma-1* transcriptional reporter in the PVD cell body at the early L3 stage showed that *dma-1* transcription was also significantly increased in the *lin-14(n179rf)* mutants compared with wild-type animals (Fig. 6 *F–H*), suggesting that *lin-14* negatively regulates *dma-1* expression in PVD neurons through a transcriptional means. Since the *lin-14* gene encodes a transcription factor, LIN-14 is likely to directly regulate *dma-1* expression. Consistent with this prediction, the chromatin immunoprecipitation sequencing (ChIP-seq) analysis showed direct binding of LIN-14 transcription factors to immediate upstream and downstream regions of the *dma-1* gene and its gene body (Fig. 6 *I*, *Left*). As expected, binding of LIN-14 was not detected around the *hpo-30* gene (Fig. 6 *I*, *Right*). To further strengthen the relationship between the *lin-4-lin-14* regulatory circuit and *dma-1* in the context of dendrite growth ability, we analyzed dendrite outgrowth in *dma-1(xr50lf); lin-14(n179rf)* double mutants versus *lin-14(n179rf)* and *dma-1(xr50lf)* single mutants. The *dma-1(xr50)* allele, containing a c-to-t missense mutation that results in an L/F change at aa137, shows limited PVD dendrite outgrowth similar to the null allele. The *dma-1(xr50lf)* mutation significantly suppressed the excessive tertiary dendrite outgrowth caused by the *lin-14(n179rf)* mutation (Fig. 6*J*). Taken together, these results indicate that the *lin-4-lin-14* regulatory circuit promotes dendrite outgrowth through transcriptional up-regulation of the DMA-1 receptor level on dendrites (Fig. 7*H*).

To determine whether the *lin-28-let-7-lin-41* regulatory circuit also controls the timing of PVD dendrite arborization

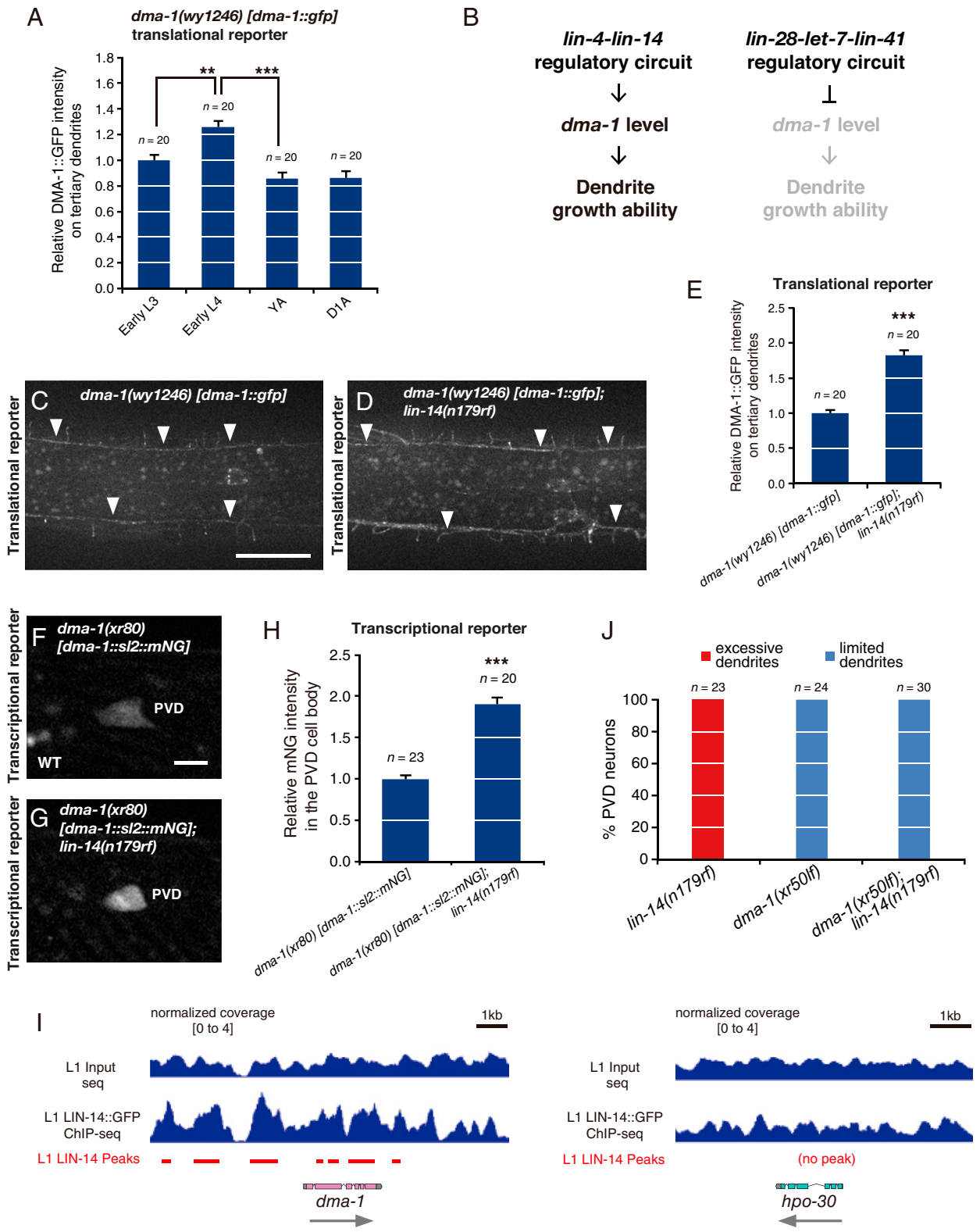

Fig. 6. *lin-14* negatively regulates DMA-1 protein levels on PVD dendrites through a transcriptional means. (*A*) Average fluorescence intensity of DMA-1::GFP fusion proteins on PVD tertiary dendrites at different stages. Error bars, SEM. $^{**}P < 0.01$ and $^{***}P < 0.001$ by one-way ANOVA with Tukey's test. (*B*) Model of temporal control of PVD dendrite growth ability through antagonistic regulation of *dma-1* by two microRNA regulatory circuits. (*C* and *D*) Representative images showing the expression of endogenous DMA-1::GFP fusion proteins on PVD dendrites in the wild type (*C*) and the *lin-14(n179rf)* mutant (*D*) at the early L4 stage. Arrowheads point to tertiary dendrites. Dorsal is *Up*; anterior is to the *Left*. Scale bar, 20 μm. (*E*) Average fluorescence intensity of DMA-1::GFP fusion proteins on PVD tertiary dendrites in the wild type versus *lin-14(n179rf)* mutants at the early L4 stage. Error bars, SEM. $^{***}P < 0.001$ by a Student's *t* test. (*F* and *G*) Representative images showing expression of the SL2-based *dma-1* transcriptional reporter in PVD neurons in the wild type (*F*) and the *lin-14(n179rf)* mutant (*G*) at the early L3 stage. Scale bar, 5 μm. (*H*) Average fluorescence intensity of the SL2-based *dma-1* transcriptional reporter in the PVD soma in the wild type versus *lin-14(n179rf)* mutants at the early L3 stage. Error bars, SEM. $^{***}P < 0.001$ by a Student's *t* test. (*I*) LIN-14 ChIP-seq binding at the *dma-1* gene (*Left*) and the *hpo-30* gene (*Right*). Tracks from IGV are shown for inputs and ChIP samples. Significant LIN-14 peaks shown in red lines below the ChIP-seq tracks were called by MACS2 (69). (*J*) Percentages of PVD neurons at the young adult stage with excessive or limited tertiary dendrite outgrowth in various strains. All strains in *C* to *H* and *J* were raised at 25 °C, which is a nonpermissive temperature for the *lin-14(n179)* allele.

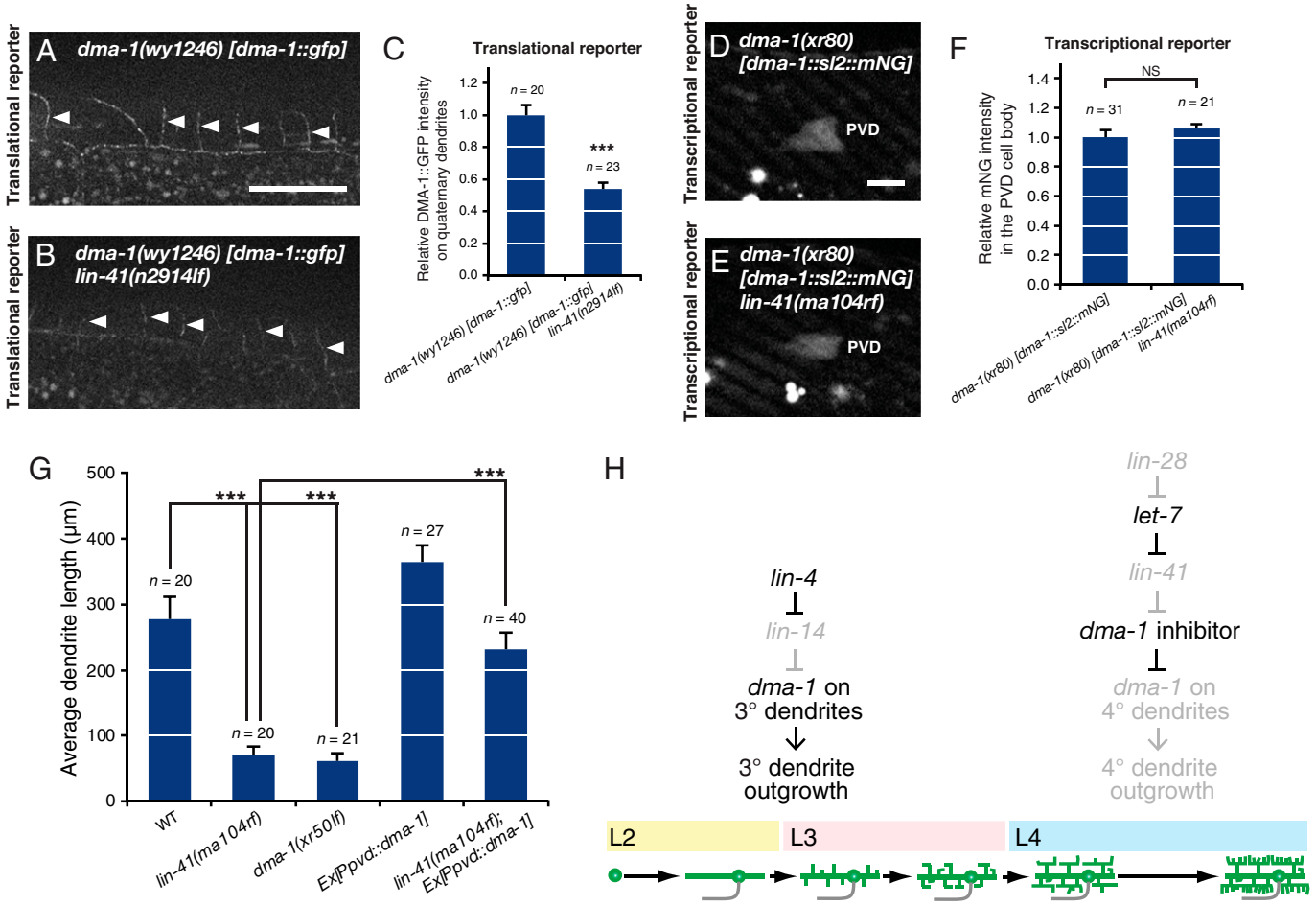

Fig. 7. *lin-41* positively regulates DMA-1 protein levels on PVD dendrites through a posttranscriptional means. (*A* and *B*) Representative images showing the expression of endogenous DMA-1::GFP fusion proteins on PVD dendrites in the wild type (*A*) and the *lin-41(n2914lf)* mutant (*B*) at the young adult stage. Arrowheads point to quaternary dendrites. Dorsal is *Up*; anterior is to the *Left*. Scale bar, 20 μm. (*C*) Average fluorescence intensity of DMA-1::GFP fusion proteins on PVD quaternary dendrites in the wild type versus *lin-41(n2914lf)* mutants at the young adult stage. Error bars, SEM. ***$P < 0.001$ by a Student's *t* test. (*D* and *E*) Representative images showing expression of the SL2-based *dma-1* transcriptional reporter in PVD neurons in the wild type (*D*) and the *lin-41(ma104rf)* mutant (*E*) at the early L3 stage. Scale bar, 5 μm. (*F*) Average fluorescence intensity of the SL2-based *dma-1* transcriptional reporter in the PVD soma in the wild type versus *lin-41(ma104rf)* mutants at the early L3 stage. Error bars, SEM. NS, not significant by a Student's *t* test. (*G*) Average PVD dendrite length regrown in various strains 24 h following dendritomy of the primary dendrite at the young adult stage. Error bars, SEM. ***$P < 0.001$ by one-way ANOVA with Tukey's test. (*H*) Model of regulation of dendritic arborization by two timing circuits. Initially, the *lin-4* microRNA down-regulates *lin-14* to trigger dendrite arborization. Later, the *let-7* microRNA down-regulates *lin-41* to slow down dendrite growth in the final stage of dendrite arborization.

through the regulation of the DMA-1 receptor level on PVD dendrites, we analyzed the level of DMA-1 proteins on quaternary dendrites in *lin-41(n2914lf)* mutants versus wild-type animals. The endogenous level of DMA-1 proteins was significantly reduced in *lin-41(n2914lf)* mutants (Fig. 7 *A*–*C*), consistent with their lower dendrite growth ability (Fig. 3*F*). This result suggests that *lin-41* positively regulates the DMA-1 protein level on PVD dendrites. To understand the mechanism by which *lin-41* positively regulates *dma-1* expression, we analyzed expression of the SL2-based *dma-1* transcriptional reporter in the PVD cell body in *lin-41(ma104rf)* mutants versus the wild type at the early L3 stage. The *lin-41(ma104rf)* mutation did not affect *dma-1* transcription, suggesting that *lin-41* positively regulates the DMA-1 protein level on PVD dendrites through a posttranscriptional means (Fig. 7 *D*–*F*). Considering that the known role of LIN-41, either as an RNA-binding protein or a ubiquitin ligase, is to negatively regulate target gene expression (15, 22, 25, 55), LIN-41 most likely positively regulates the DMA-1 level through an indirect mechanism such as negative regulation of a *dma-1* inhibitor (Fig. 7*H*). To further strengthen the relationship between the *lin-28-let-7-lin-41* regulatory circuit and *dma-1* in the context of dendrite growth ability, we performed laser dendritomy on the PVD primary dendrite in *lin-41(ma104rf)* mutants with or without *dma-1* overexpression in PVD neurons at the young adult stage. *dma-1* overexpression in PVD neurons significantly suppressed the reduced dendrite growth ability caused by the *lin-41(ma104rf)* mutation (Fig. 7*G*). This result indicates that the *lin-28-let-7-lin-41* regulatory circuit inhibits dendrite growth ability through posttranscriptional down-regulation of the DMA-1 receptor level on dendrites (Fig. 7*H*). Taken together, our findings support a model in which the *lin-4-lin-14* and the *lin-28-let-7-lin-41* regulatory circuits control the timing of PVD dendrite arborization through antagonistic regulation of the DMA-1 receptor level on dendrites (Fig. 7*H*). The LIN-14 transcription factor likely acts directly to transcriptionally repress *dma-1* expression, whereas the LIN-41 tripartite motif protein likely acts indirectly to posttranscriptionally promote *dma-1* expression in PVD neurons.

A candidate gene that can act between *lin-41* and *dma-1* in PVD neurons is the *lin-29* zinc finger transcription factor as it is a known *lin-41* target gene and is expressed in PVD nuclei (*SI Appendix*, Fig. S7 *A* and *C*). *lin-29* has been reported to be negatively regulated by *lin-41* in certain cellular contexts (15, 22, 25, 55). Although the LIN-29 transcription factor is

expressed in PVD nuclei strongly from the L4 stage onwards (*SI Appendix*, Fig. S7*A*), the *lin-29(n333lf)* mutation did not affect *dma-1* transcription (*SI Appendix*, Fig. S7*B*), suggesting that *lin-29* is unlikely to regulate *dma-1* expression in PVD neurons. To further assess whether *lin-29* acts as a *dma-1* inhibitor in PVD neurons (Fig. 7*H*), we examined the effect of *lin-29* deficiency on PVD dendrite growth ability. Using the ZIF-1-mediated protein degradation system to deplete LIN-29 proteins specifically in PVD neurons (56, 57), we found that the PVD-specific LIN-29 knockdown did not affect PVD dendrite growth ability at the young adult stage (*SI Appendix*, Fig. S7 *C* and *D*), further supporting the notion that *lin-29* is unlikely to act between *lin-41* and *dma-1* to control the timing of PVD dendrite arborization.

Discussion

In this report, we show that two microRNA regulatory circuits are used in timing dendritic arborization in postmitotic PVD neurons, restricting dendrite growth within a defined time frame. The precisely timed *lin-4-lin-14* regulatory circuit sets off initial dendrite outgrowth until the L4 stage, at which the precisely timed *lin-28-let-7-lin-41* regulatory circuit decelerates dendrite growth as terminal dendrite branches are reaching final targets (Fig. 7*H*). These two regulatory circuits control the timing of PVD dendrite arborization through opposed regulation of the DMA-1 receptor level on PVD dendrites (Fig. 7*H*).

The neuronal timers that restrain dendrite arborization within a specific time window during neural circuit formation are poorly understood and remain a mystery. In this study, we uncover two microRNA regulatory circuits that temporally control the choreography of dendrite arborization in PVD neurons. Our study illustrates how neuronal timers regulate the intrinsic potential of dendrite growth. From this point forward, our goal is to describe the required timing mechanisms in dendritic arborization at a resolution that ultimately will allow us to reconstitute the process. Further dissection of genetic networks that regulate the timing of *lin-4* and *let-7* expression and identification of the downstream target of the LIN-41 tripartite motif protein that regulates the DMA-1 receptor level on dendrites will be indispensable to achieving this goal.

Here, we show that the *lin-4-lin-14* regulatory circuit initiates PVD dendrite arborization through up-regulation of the DMA-1 receptor level on dendrites. The LIN-14 transcription factor most likely binds to the cis-regulatory region of the *dma-1* gene to negatively regulate *dma-1* transcription (Fig. 6 *F*–*I*). We also report that the *lin-28-let-7-lin-41* regulatory circuit slows down PVD dendrite arborization as it comes to an end through down-regulation of the DMA-1 receptor level on dendrites. The positive regulation of the DMA-1 level by LIN-41 is likely indirect since LIN-41 is known to negatively regulate its target genes (15, 22, 25, 55). The LIN-41 tripartite motif protein is proposed to negatively regulate a *dma-1* inhibitor to posttranscriptionally promote the DMA-1 receptor level on PVD dendrites (Fig. 7 *D*–*F* and *H*).

In this study, we show that *lin-4(e912lf)*, *lin-14(n355gf)*, and *dma-1(xr50lf)* mutants display a similar phenotype of limited PVD dendrite outgrowth at the young adult stage (Fig. 2 *A*–*C*, *E*, and Fig. 6*J*). The frequency of the PVD secondary branches in *dma-1(xr50lf)* mutants was 35% lower compared with that in the wild type but was similar to the extent of phenotypes observed in *lin-4(e912lf)* and *lin-14(n355gf)* mutants. This observation further supports our model in which the LIN-14 transcription factor represses the *dma-1* gene expression to control the timing of PVD dendrite arborization. Furthermore, even at the young adult stage, only subsets of PVD neurons in *lin-4(e912lf)* and *lin-14(n355gf)* mutants display a small number of tertiary branches in the area close to the cell body but rarely any in the distal area. This polarity in the tertiary dendrite outgrowth seems to be less noticeable in *dma-1(xr50lf)* mutants. A possible explanation is that, in *lin-4(e912lf)* and *lin-14(n355gf)* mutants, fewer DMA-1 proteins are generated in the cell body so while some tertiary dendrite outgrowth can still be supported in the area proximal to the cell body, much less DMA-1 proteins are transported to the distal area to support tertiary dendrite outgrowth.

A previous study has reported that PVD neurons display progressive morphological changes as they age into adulthood, including dendrite hyperbranching, which is disorganized and distinct from stereotyped dendrite branching in early development (58). Dendrite hyperbranching in aged neurons is likely caused by disorganization of dendrite cytoskeletons and does not reflect dendrite growth ability. Indeed, consistent with our findings, Kravtsov et al. (58) have reported a lower dendrite growth ability during the regeneration of PVD neurons in older animals than younger animals.

In the *let-7(xr67)* CRISPR line, the *let-7* microRNA expressed from the *lin-4* upstream sequence does not block PVD dendrite growth in early development. This could be due to many different reasons. For example, the *lin-4* upstream sequence::*let-7* genomic configuration may not be able to support the expression and processing of the primary *let-7* microRNA as efficiently as the *lin-4* upstream sequence::*lin-4* genomic configuration supports the expression and processing of the primary *lin-4* microRNA. Alternatively, between the *lin-4-lin-14* and the *let-7-lin-41* regulatory circuits, the *lin-4-lin-14* regulatory circuit could impact the DMA-1 receptor level to a larger extent than the *let-7-lin-41* regulatory circuit.

It remains to be seen whether the timing of dendrite arborization by *lin-4* and *let-7* microRNA regulatory circuits can be extended beyond PVD neurons, especially knowing that these two timing microRNAs are expressed broadly in many neurons in *C. elegans* (*SI Appendix*, Fig. S1 *A*–*F*) (24–26). Since *let-7* and *lin-4* microRNAs are evolutionarily conserved, it is possible that these microRNA regulatory circuits control the timing of dendrite arborization in other organisms as well. This possibility is supported by the findings that *let-7* is expressed in the nervous system in various species, including *C. elegans*, *Drosophila*, mouse, and human (21, 25, 59, 60) and that *miR-125*, the *lin-4* homolog, functions in the *Drosophila* and mouse nervous system (61, 62). Although the timing of dendrite arborization is less understood in vertebrates, untimely dendrite arborization would likely lead to neurodevelopmental and psychiatric disorders that are frequently associated with defective dendritic arbors (63).

In this study, we discover a role for the *lin-4-lin-14* and the *lin-28-let-7-lin-41* regulatory circuits in temporal control of PVD dendrite arborization. We do not rule out the possibility that these microRNA regulatory circuits may also be involved in other differentiation events in PVD neurons. Indeed, using a PVD neuronal marker to assess its differentiation state in *lin-14(n179rf)* mutants, we found that PVD neurons in *lin-14(n179rf)* mutants exhibit precocious differentiation (*SI Appendix*, Fig. S8), suggesting that the timing of many differentiation events in PVD may also be controlled by the *lin-4-lin-14* regulatory circuit.

Materials and Methods

Strains and Plasmids. Strains and plasmids used in this study are listed in *SI Appendix*, Tables S1 and S2.

CRISPR-Cas9 Genome Editing. We generated the *lin-4(xr70)*, *lin-4(xr71)*, *let-7(xr67)*, *let-7(xr68)*, *dma-1(wy1246)*, and *dma-1(xr80)* CRISPR alleles using the CRISPR-Cas9 genome editing technology. CRISPR recombinants were identified using a self-excising drug selection cassette as previously described (44, 45). The strategies to build the *lin-4(xr70)*, *lin-4(xr71)*, *let-7(xr67)*, and *let-7(xr68)* alleles are illustrated in the diagrams in Figs. 4*A*′ and 5*A*′. In our upstream sequence swap experiments, we swapped between the 2.9-kb sequence upstream of *let-7* premature-microRNA (pre-miRNA) and the 1.9-kb sequence upstream of *lin-4* pre-miRNA. In the upstream sequence, it contains temporal information for both driving microRNA expression and processing primary microRNA. The *dma-1(wy1246)[dma-1::gfp]* allele was built by inserting a GFP reporter gene after the transmembrane domain of the endogenous *dma-1* gene. This knock-in strain does not show any noticeable defects in PVD dendrites. The *dma-1(xr80)[dma-1::sl2::mNG]* transcriptional reporter allele was built by inserting the SL2 trans-splice site and the mNG reporter gene into the 3′ end of the endogenous *dma-1* gene.

Stem-Loop RT-PCR. We evaluated the change of the mature *lin-4* and *let-7* microRNA levels during development by modifying the microRNA assay developed previously (25, 64). Equal amounts of the RNA preparation from staged wild type, *lin-4(xr71)*, and *let-7(xr67)* animals were used for RT-PCR amplification of mature microRNAs and of *pmp-3* transcripts. Next, a 50 nM stem-loop (for *lin-4* and *let-7* microRNAs) or regular (for *pmp-3*) RT primer was used in reverse transcription reactions. The mixture of RNA template, dNTPs, and RT primer was incubated for 5 min at 65 °C. The mixture was then placed on ice for at least 1 min before adding RT buffer, DTT, $MgCl_2$, SuperScript III, and RNase inhibitor. The reaction was incubated for 50 min at 50 °C before heat inactivation at 85 °C for 5 min. PCR was conducted using 0.25 μL RT products as the template in a 20-μL PCR solution for 17 cycles.

Laser Dendritomy. Animals were mounted on 2% agarose pads and anesthetized with 5 mM sodium azide, the lowest possible concentration to keep adult animals immobilized. Laser dendritomy was performed on PVD primary dendrites in worms at the young adult stage unless otherwise described. Either a cavity-dumped Ti:sapphire laser oscillator (Cascade Laser, KMLabs Inc.) (65) or a MicroPoint Laser Ablation System (Andor/Oxford Instruments) was used for dendritomy. The laser pulses were tightly focused onto targeted primary dendrites using a Plan Apo VC 100×, 1.4 numerical aperture oil-immersion objective on a Nikon ECLIPSE Ti microscope. Successful laser dendritomy was confirmed by visualizing the targeted area immediately after surgery. Worms were recovered within 10 min of sodium azide treatment and placed on fresh plates with bacterial food.

Quantification of Dendrite Lengths. PVD neurons in recovered worms were imaged 24 h after dendritomy, and the dendrite regrowth was quantified. Dendrite lengths were calculated as the actual contour length between the injury site and dendrite termini measured along the cylindrical surface of each worm by tracing dendrites through a 3-dimensional image stack.

Quantification of the DMA-1::GFP Intensity. DMA-1::GFP intensities on tertiary (or quaternary) dendrite branches were quantified using the ImageJ software. DMA-1::GFP intensities on different tertiary (or quaternary) dendrite branches in a given PVD neuron were rather similar. Five tertiary (or quaternary) dendrite branches were randomly selected in each PVD neuron, and a single focal plane that contained a selected branch in focus was used for each measurement. Overlapping regions of tertiary dendrite branches in *lin-14(n179rf)* mutants were avoided during the analysis. For each dendrite branch, a region of interest was selected using the Line Selection Tool, and the Mean Gray Value was measured using the Measure function, followed by background subtraction. Intensity values for five branches were averaged for each PVD neuron, and the mean signal intensity and the corresponding SEM were calculated for each genotype.

ChIP-seq and Analysis. The LIN-14::GFP ChIP-seq track for *dma-1* and *hpo-30* were analyzed from the dataset in Sun and Hobert (66). The C-terminally GFP-tagged *lin-14* (*lin-14(cc2841)[lin-14::gfp]*) strain was used for the ChIP-seq analysis. Around 600,000 L1 animals were collected and fixed with 2% formaldehyde for 15 min at room temperature. The ChIP-seq analysis was performed as previously described (66). The immunoprecipitated DNA was purified using Ampure XP beads (A63881) and used to generate a sequencing library using the Ovation Ultralow System V2 (Tecan) according to the manufacturer's instructions. The libraries were sequenced on Illumina NextSeq 500 machines with 75-bp single-end reads. After an initial quality check, the reads were mapped to WS220 using BWA (67) and filtered using SAMtools (68). Peaks were called using MACS2 (69) and visualized using IGV. All peaks and differential binding sites were annotated and assigned to the nearest gene using ChIPseeker (70). Detailed descriptions of the quality check and validation of the ChIP-seq data set were described in Sun and Hobert (66). Briefly, GFP ChIP-seq from the LIN-14::GFP strain showed appreciable enrichment over input as well as GFP ChIP-seq from N2 controls. Additionally, the ChIP-seq data matched well with the expression pattern and function of LIN-14 across development, as well as validated expression change of LIN-14 targets.

Statistical Analysis. Statistical analyses were carried out by Student's *t* tests, two-proportion *Z*-tests, or one-way ANOVA with Tukey's or Dunnett's tests using GraphPad Prism 7.0 or the Primer of Biostatistics software.

Data, Materials, and Software Availability. All study data are included in the article and/or *SI Appendix*.

ACKNOWLEDGMENTS. This work was funded by grants from the NSF (IOS-1455758 to C.C.), the National Institute of General Medical Sciences of the NIH (R01GM111320 to C.C.), and the Howard Hughes Medical Institute (to K.S.). We thank Oliver Hobert for the *lin-29(xe61)* strain; Hui Chiu for critical reading of the manuscript, providing critical initial data, and making figures; Daniel J. Dickinson and Bob Goldstein for providing reagents and CRISPR protocols; David H. A. Fitch for the *lep-5(ny28)* allele; Daniel D. Shaye and Chiou-Fen Chuang for constructs and critical comments; the *Caenorhabditis* Genetics Center for strains; and the WormBase for readily accessible information.

1. T. A. Bargiello, F. R. Jackson, M. W. Young, Restoration of circadian behavioural rhythms by gene transfer in *Drosophila*. *Nature* **312**, 752–754 (1984).
2. J. Cooke, E. C. Zeeman, A clock and wavefront model for control of the number of repeated structures during animal morphogenesis. *J. Theor. Biol.* **58**, 455–476 (1976).
3. P. E. Hardin, J. C. Hall, M. Rosbash, Feedback of the *Drosophila* period gene product on circadian cycling of its messenger RNA levels. *Nature* **343**, 536–540 (1990).
4. K. Horikawa, K. Ishimatsu, E. Yoshimoto, S. Kondo, H. Takeda, Noise-resistant and synchronized oscillation of the segmentation clock. *Nature* **441**, 719–723 (2006).
5. T. Kondo, A cyanobacterial circadian clock based on the Kai oscillator. *Cold Spring Harb. Symp. Quant. Biol.* **72**, 47–55 (2007).
6. X. Liu *et al.*, The period gene encodes a predominantly nuclear protein in adult *Drosophila*. *J. Neurosci.* **12**, 2735–2744 (1992).
7. D. O. Morgan, Cyclin-dependent kinases: Engines, clocks, and microprocessors. *Annu. Rev. Cell Dev. Biol.* **13**, 261–291 (1997).
8. M. Nakajima *et al.*, Reconstitution of circadian oscillation of cyanobacterial KaiC phosphorylation in vitro. *Science* **308**, 414–415 (2005).
9. A. C. Oates, L. G. Morelli, S. Ares, Patterning embryos with oscillations: Structure, function and dynamics of the vertebrate segmentation clock. *Development* **139**, 625–639 (2012).
10. J. L. Price *et al.*, double-time is a novel *Drosophila* clock gene that regulates PERIOD protein accumulation. *Cell* **94**, 83–95 (1998).
11. S. M. Reppert, D. R. Weaver, Coordination of circadian timing in mammals. *Nature* **418**, 935–941 (2002).
12. K. K. Siwicki, C. Eastman, G. Petersen, M. Rosbash, J. C. Hall, Antibodies to the period gene product of *Drosophila* reveal diverse tissue distribution and rhythmic changes in the visual system. *Neuron* **1**, 141–150 (1988).
13. L. B. Vosshall, J. L. Price, A. Sehgal, L. Saez, M. W. Young, Block in nuclear localization of period protein by a second clock mutation, timeless. *Science* **263**, 1606–1609 (1994).
14. W. A. Zehring *et al.*, P-element transformation with period locus DNA restores rhythmicity to mutant, arrhythmic *Drosophila melanogaster*. *Cell* **39**, 369–376 (1984).
15. L. Pereira *et al.*, Timing mechanism of sexually dimorphic nervous system differentiation. *eLife* **8**, e42078 (2019).
16. F. Faunes, J. Larraín, Conservation in the involvement of heterochronic genes and hormones during developmental transitions. *Dev. Biol.* **416**, 3–17 (2016).
17. A. E. Rougvie, E. G. Moss, Developmental transitions in *C. elegans* larval stages. *Curr. Top. Dev. Biol.* **105**, 153–180 (2013).
18. R. C. Lee, R. L. Feinbaum, V. Ambros, The *C. elegans* heterochronic gene lin-4 encodes small RNAs with antisense complementarity to lin-14. *Cell* **75**, 843–854 (1993).
19. B. Wightman, I. Ha, G. Ruvkun, Posttranscriptional regulation of the heterochronic gene lin-14 by lin-4 mediates temporal pattern formation in *C. elegans*. *Cell* **75**, 855–862 (1993).
20. R. Feinbaum, V. Ambros, The timing of lin-4 RNA accumulation controls the timing of postembryonic developmental events in *Caenorhabditis elegans*. *Dev. Biol.* **210**, 87–95 (1999).
21. A. E. Pasquinelli *et al.*, Conservation of the sequence and temporal expression of let-7 heterochronic regulatory RNA. *Nature* **408**, 86–89 (2000).
22. F. J. Slack *et al.*, The lin-41 RBCC gene acts in the *C. elegans* heterochronic pathway between the let-7 regulatory RNA and the LIN-29 transcription factor. *Mol. Cell* **5**, 659–669 (2000).

23. B. J. Reinhart *et al.*, The 21-nucleotide let-7 RNA regulates developmental timing in *Caenorhabditis elegans*. *Nature* **403**, 901–906 (2000).
24. Y. Zou, H. Chiu, D. Domenger, C. F. Chuang, C. Chang, The lin-4 microRNA targets the LIN-14 transcription factor to inhibit netrin-mediated axon attraction. *Sci. Signal.* **5**, ra43 (2012).
25. Y. Zou *et al.*, Developmental decline in neuronal regeneration by the progressive change of two intrinsic timers. *Science* **340**, 372–376 (2013).
26. M. Shih, C. Chang, Brain-wide identification of LIN-41 (TRIM71) protein-expressing neurons by NeuroPAL. *MicroPubl. Biol.* **2021**, 10.17912/micropub.biology.000472 (2021).
27. H. Chiu, A. Alqadah, C. Chang, The role of microRNAs in regulating neuronal connectivity. *Front. Cell. Neurosci.* **7**, 283 (2014).
28. K. Olsson-Carter, F. J. Slack, A developmental timing switch promotes axon outgrowth independent of known guidance receptors. *PLoS Genet.* **6**, e1001054 (2010).
29. Y. Xu, C. C. Quinn, Transition between synaptic branch formation and synaptogenesis is regulated by the lin-4 microRNA. *Dev. Biol.* **420**, 60–66 (2016).
30. S. J. Hallam, Y. Jin, lin-14 regulates the timing of synaptic remodelling in *Caenorhabditis elegans*. *Nature* **395**, 78–82 (1998).
31. K. Howell, J. G. White, O. Hobert, Spatiotemporal control of a novel synaptic organizer molecule. *Nature* **523**, 83–87 (2015).
32. O. Aurelio, T. Boulin, O. Hobert, Identification of spatial and temporal cues that regulate postembryonic expression of axon maintenance factors in the *C. elegans* ventral nerve cord. *Development* **130**, 599–610 (2003).
33. H. Chiu, C. Chang, Rejuvenating nerve cells in adults. *Aging (Albany NY)* **5**, 485–486 (2013).
34. M. Armakola, G. Ruvkun, Regulation of *Caenorhabditis elegans* neuronal polarity by heterochronic genes. *Proc. Natl. Acad. Sci. U.S.A.* **116**, 12327–12336 (2019).
35. L. Sundararajan, J. Stern, D. M. Miller III, Mechanisms that regulate morphogenesis of a highly branched neuron in *C. elegans*. *Dev. Biol.* **451**, 53–67 (2019).
36. S. Inberg *et al.*, Lessons from worm dendritic patterning. *Annu. Rev. Neurosci.* **42**, 365–383 (2019).
37. O. W. Liu, K. Shen, The transmembrane LRR protein DMA-1 promotes dendrite branching and growth in *C. elegans*. *Nat. Neurosci.* **15**, 57–63 (2011).
38. N. J. Lehrbach *et al.*, LIN-28 and the poly(U) polymerase PUP-2 regulate let-7 microRNA processing in *Caenorhabditis elegans*. *Nat. Struct. Mol. Biol.* **16**, 1016–1020 (2009).
39. B. Vadla, K. Kemper, J. Alaimo, C. Heine, E. G. Moss, lin-28 controls the succession of cell fate choices via two distinct activities. *PLoS Genet.* **8**, e1002588 (2012).
40. P. M. Van Wynsberghe *et al.*, LIN-28 co-transcriptionally binds primary let-7 to regulate miRNA maturation in *Caenorhabditis elegans*. *Nat. Struct. Mol. Biol.* **18**, 302–308 (2011).
41. S. R. Viswanathan, G. Q. Daley, R. I. Gregory, Selective blockade of microRNA processing by Lin28. *Science* **320**, 97–100 (2008).
42. K. C. Kiontke *et al.*, The long non-coding RNA lep-5 promotes the juvenile-to-adult transition by destabilizing LIN-28. *Dev. Cell* **49**, 542–555.e9 (2019).
43. H. Lawson *et al.*, The Makorin *lep-2* and the lncRNA *lep-5* regulate *lin-28* to schedule sexual maturation of the *C. elegans* nervous system. *eLife* **8**, e43660 (2019).
44. D. J. Dickinson, A. M. Pani, J. K. Heppert, C. D. Higgins, B. Goldstein, Streamlined genome engineering with a self-excising drug selection cassette. *Genetics* **200**, 1035–1049 (2015).
45. D. J. Dickinson, J. D. Ward, D. J. Reiner, B. Goldstein, Engineering the *Caenorhabditis elegans* genome using Cas9-triggered homologous recombination. *Nat. Methods* **10**, 1028–1034 (2013).
46. C. A. Díaz-Balzac *et al.*, Muscle- and skin-derived cues jointly orchestrate patterning of somatosensory dendrites. *Curr. Biol.* **26**, 2379–2387 (2016).
47. X. Dong, O. W. Liu, A. S. Howell, K. Shen, An extracellular adhesion molecule complex patterns dendritic branching and morphogenesis. *Cell* **155**, 296–307 (2013).
48. Y. Salzberg *et al.*, Skin-derived cues control arborization of sensory dendrites in *Caenorhabditis elegans*. *Cell* **155**, 308–320 (2013).
49. W. Zou *et al.*, A multi-protein receptor-ligand complex underlies combinatorial dendrite guidance choices in *C. elegans*. *eLife* **5**, e18345 (2016).
50. X. Dong *et al.*, Precise regulation of the guidance receptor DMA-1 by KPC-1/Furin instructs dendritic branching decisions. *eLife* **5**, e11008 (2016).
51. C. J. Smith *et al.*, Sensory neuron fates are distinguished by a transcriptional switch that regulates dendrite branch stabilization. *Neuron* **79**, 266–280 (2013).
52. W. Zou *et al.*, A dendritic guidance receptor complex brings together distinct actin regulators to drive efficient F-actin assembly and branching. *Dev. Cell* **45**, 362–375.e3 (2018).
53. L. T. Tang *et al.*, TIAM-1/GEF can shape somatosensory dendrites independently of its GEF activity by regulating F-actin localization. *eLife* **8**, e38949 (2019).
54. B. Tursun, L. Cochella, I. Carrera, O. Hobert, A toolkit and robust pipeline for the generation of fosmid-based reporter genes in *C. elegans*. *PLoS One* **4**, e4625 (2009).
55. F. Aeschimann *et al.*, LIN41 Post-transcriptionally Silences mRNAs by Two Distinct and Position-Dependent Mechanisms. *Mol. Cell* **65**, 476–489.e4 (2017).
56. S. T. Armenti, L. L. Lohmer, D. R. Sherwood, J. Nance, Repurposing an endogenous degradation system for rapid and targeted depletion of *C. elegans* proteins. *Development* **141**, 4640–4647 (2014).
57. S. Wang *et al.*, A toolkit for GFP-mediated tissue-specific protein degradation in *C. elegans*. *Development* **144**, 2694–2701 (2017).
58. V. Kravtsov, M. Oren-Suissa, B. Podbilewicz, The fusogen AFF-1 can rejuvenate the regenerative potential of adult dendritic trees by self-fusion. *Development* **144**, 2364–2374 (2017).
59. C. L. A. Fairchild *et al.*, Let-7 regulates cell cycle dynamics in the developing cerebral cortex and retina. *Sci. Rep.* **9**, 15336 (2019).
60. L. F. Sempere, E. B. Dubrovsky, V. A. Dubrovskaya, E. M. Berger, V. Ambros, The expression of the let-7 small regulatory RNA is controlled by ecdysone during metamorphosis in *Drosophila melanogaster*. *Dev. Biol.* **244**, 170–179 (2002).
61. M. Åkerblom *et al.*, microRNA-125 distinguishes developmentally generated and adult-born olfactory bulb interneurons. *Development* **141**, 1580–1588 (2014).
62. Y. C. Wu, C. H. Chen, A. Mercer, N. S. Sokol, Let-7-complex microRNAs regulate the temporal identity of *Drosophila* mushroom body neurons via chinmo. *Dev. Cell* **23**, 202–209 (2012).
63. A. J. Koleske, Molecular mechanisms of dendrite stability. *Nat. Rev. Neurosci.* **14**, 536–550 (2013).
64. C. Chen *et al.*, Real-time quantification of microRNAs by stem-loop RT-PCR. *Nucleic Acids Res.* **33**, e179 (2005).
65. H. Chiu *et al.*, Engulfing cells promote neuronal regeneration and remove neuronal debris through distinct biochemical functions of CED-1. *Nat. Commun.* **9**, 4842 (2018).
66. H. Sun, O. Hobert, Temporal transitions in the post-mitotic nervous system of *Caenorhabditis elegans*. *Nature* **600**, 93–99 (2021).
67. H. Li, R. Durbin, Fast and accurate short read alignment with Burrows-Wheeler transform. *Bioinformatics* **25**, 1754–1760 (2009).
68. H. Li *et al.*; 1000 Genome Project Data Processing Subgroup, The sequence alignment/map format and SAMtools. *Bioinformatics* **25**, 2078–2079 (2009).
69. J. Feng, T. Liu, B. Qin, Y. Zhang, X. S. Liu, Identifying ChIP-seq enrichment using MACS. *Nat. Protoc.* **7**, 1728–1740 (2012).
70. G. Yu, L. G. Wang, Q. Y. He, ChIPseeker: An R/Bioconductor package for ChIP peak annotation, comparison and visualization. *Bioinformatics* **31**, 2382–2383 (2015).